NUCL SCI TECH (2022) 33:134
https://doi.org/10.1007/s41365-022-01108-9

Thermal hydraulic characteristics of helical coil once-through steam generator under ocean conditions

Tian-Ze Bai[1] · Chang-Hong Peng[1]

Received: 22 June 2022 / Revised: 29 July 2022 / Accepted: 10 August 2022 / Published online: 18 October 2022

Abstract Owing to its advantages of high heat transfer efficiency and compactness, the helical coil once-through steam generator (HCOTSG) can be used in floating nuclear power plants and has been widely used in the design of small modular reactors. The helical tubular geometric structure of the HCOTSG allows heat transfer and local flow changes to occur under complex ocean conditions. In this study, theoretical models of ocean conditions are added to the RELAP5/MOD3.3 code and verified. Using the modified RELAP5 code, the thermal–hydraulic characteristics of the HCOTSG under ocean conditions are simulated. The results show that under rolling conditions, the flow oscillation amplitudes of the single liquid-phase, two-phase flow, and single gas-phase regions are different. A circular change in the horizontal position of the helical tube causes the fluctuation of the parameters to change periodically. A phase difference of approximately 3.9 s at a flow rate of 23 kg/s is observed in the flow fluctuation along the axial direction. The driving force, period, and amplitude of rolling significantly affect the flow fluctuation in the HCOTSG. In natural circulation, the flow in the HCOTSG is complex, and the primary-side flow fluctuation can reduce the trough of the flow oscillation at the helical tube by approximately 24.3%.

Keywords RELAP5 · HCOTSG · Ocean conditions · Thermal–hydraulic analysis · Flow oscillation

✉ Chang-Hong Peng
pengch@ustc.edu.cn

1 School of Nuclear Science and Technology, University of Science and Technology of China, No. 96, Jinzhai Road, Baohe District, Hefei 230026, China

1 Introduction

Floating nuclear power plants (FNPPs) have garnered increasing attention as they can be used to provide continuous, reliable, and effective power to offshore oil exploitation platforms and remote islands, as well as for seawater desalination [1]. They offer the advantages of mobility, clean environmental protection, sustainable energy supply, and insignificant land uptake [2]. In 2020, the Akademik Lomonosov offshore floating nuclear power plant in Russia was constructed for power generation [3]. Higher requirements are demanded the design and size of each reactor component owing to the limited internal space of FNPPs and their inconvenient maintenance. The helical structure and flow of high-temperature and high-pressure primary coolant in the shell side can reduce the effect of stress caused by thermal expansion on the steam generator (SG), thus improving the reliability and safety of the SG [4]. HCOTSGs feature a compact structure, a larger heat transfer area, and higher heat transfer efficiency than the U-tube and once-through SGs [5]. Therefore, HCOTSGs are an appropriate candidate for FNPPs.

Owing to the effects of ocean conditions, such as waves and winds, FNPPs can generate different types of ship motions, thus resulting in complex changes in the thermal–hydraulic characteristics of the reactor. Ship motion can be summarized into three basic motion forms: linear motion, inclining, and rotation [6]. Researchers have investigated the effects of ocean conditions on thermal–hydraulic characteristics under forced and natural circulations [7–11]. Ishida first developed a system code for the thermal–hydraulic analysis of a marine reactor based on the RETRAN-02 code and performed natural circulation experiments under moving conditions for code verification [12]. Kim developed the RETRAN-03/INT code by modifying RETRAN-03 to simulate the natural circulation characteristics of ship reactors under multidimensional motions [13]. Yan and Yu improved the RELAP5/MOD3.3 code and added a new condensation heat transfer model and a rolling motion calculation model to the code to analyze the reactor thermal–hydraulic characteristics under rolling motion [14]. Gong et al. developed a PNCMC code to simulate the natural circulation of a marine reactor [15]. Cheng et al. developed a reactor simulation code under motion conditions by adding a marine condition calculation model in the RELAP5/SCDAPSIM/MOD3.4 code and established a single-phase natural circulation experimental loop for verification [16].

Cioncolini et al. established an HCOTSG equivalent model of the IRIS reactor in steady-state operation using the RELAP5 code [17]. Xu et al. developed friction factor and heat transfer coefficient models for HCOTSGs and applied them to the RELAP5 code [18]. Current investigations pertaining to SGs in reactors under ocean conditions are primarily based on once-through and U-tube SGs. Li et al. investigated the backflow characteristics of a U-tube SG under ocean conditions [19]. Yan et al. used the IRIS reactor as a research object and analyzed the effects of ocean conditions during a station blackout accident (SBO) [20]; however, a detailed analysis of the SG has not been conducted.

Researchers have extensively performed thermal–hydraulic transient analyses under ocean conditions; however, the thermal–hydraulic characteristics of HCOTSGs under ocean conditions have not been investigated. Owing to the effect of rolling motion on the gravity drive head, the flow at the HCOTSG and U-tube SG changes periodically under ocean conditions. However, because of the helical tubular geometric structure of the HCOTSG, the secondary coolant is affected by additional tangential acceleration, thus resulting in more complex changes in the heat transfer and local flow oscillation at the helical tube. In this study, theoretical models of ocean conditions were added to the RELAP5/MOD3.3 code. The modified code was verified by comparing the code calculation results with Ishida's experimental data [12]. The calculation model of the reactor HCOTSG under ocean conditions was established, in which the research object was the SG of the IRIS reactor. The effect of rolling on the thermal–hydraulic characteristics of the HCOTSG under different flow rates and the effects of different motion parameters were investigated. The flow characteristics of the HCOTSG in natural circulation under rolling motion and the effects of primary- and secondary-side coupling of the SG under rolling motion were investigated.

2 Theoretical models of ocean condition

The effects of the three basic ship motions on the reactor cooling system under ocean conditions were different. Static inclining can change the relative spatial position of the cooling system components. Meanwhile, rotational and linear motions can be simplified to simple harmonic motions. Linear motion does not change the relative spatial position of the system components but can add linear acceleration to the fluid. Rotational motion can change the relative spatial position of the components and generate additional acceleration, which affects the coolant flow.

2.1 Spatial position change

For static inclining and rotation motions, the unit vector of the spatial position of the rotation axis is set as $\vec{n} = (n_x, n_y, n_z)$, and the rotation angle is θ. Subsequently, the new spatial position vector $\vec{L_1} = (x_1, y_1, z_1)$ of the system component can be obtained by multiplying the rotation matrix by the original spatial position vector $\vec{L_0} = (x_0, y_0, z_0)$, as shown in Eq. (1).

$$\begin{bmatrix} x_1 \\ y_1 \\ z_1 \end{bmatrix} = \begin{bmatrix} n_x^2(1-\cos\theta)+\cos\theta & n_xn_y(1-\cos\theta)-n_z\sin\theta & n_xn_z(1-\cos\theta)+n_y\sin\theta \\ n_xn_y(1-\cos\theta)+n_z\sin\theta & n_y^2(1-\cos\theta)+\cos\theta & n_yn_z(1-\cos\theta)-n_x\sin\theta \\ n_xn_z(1-\cos\theta)-n_y\sin\theta & n_yn_z(1-\cos\theta)+n_x\sin\theta & n_z^2(1-\cos\theta)+\cos\theta \end{bmatrix} \begin{bmatrix} x_0 \\ y_0 \\ z_0 \end{bmatrix} \tag{1}$$

The rotation angle of the static inclination is fixed, whereas the rotation angle of the rotation motion changes with time. In general, the rotational motion can be simplified into simple harmonic motion. Therefore, the rotation angle expressed in the form of simple harmonic motion is as follows:

$$\theta = \theta_a \sin\left[\frac{2\pi}{T}(t - t_0)\right], \tag{2}$$

where T is the movement period, t_0 is the starting time, and θ_a is amplitude of rotation angle.

2.2 Additional acceleration

For linear motion in the case of simple harmonic motion, the additional acceleration $\overrightarrow{a_{\rm l}} = (a_{x,{\rm l}}, a_{y,{\rm l}}, a_{z,{\rm l}})$ can be expressed as

$$\begin{aligned} a_{x,{\rm l}} &= A_x \sin\left[\frac{2\pi}{T}(t-t_0)\right], \\ a_{y,{\rm l}} &= A_y \sin\left[\frac{2\pi}{T}(t-t_0)\right], \\ a_{z,{\rm l}} &= A_z \sin\left[\frac{2\pi}{T}(t-t_0)\right], \end{aligned} \tag{3}$$

where $A_x, A_y,$ and A_z are the amplitudes in the x-, y-, and z-directions, respectively.

Using the rotation angle of rotational motion represented in Eq. (2), the angular velocity and angular acceleration of the rotational motion are expressed as follows:

$$\omega(t) = \frac{2\pi\theta_{\rm a}}{T}\cos\left[\frac{2\pi}{T}(t-t_0)\right], \tag{4}$$

$$\beta(t) = -\frac{4\pi^2\theta_{\rm a}}{T^2}\sin\left[\frac{2\pi}{T}(t-t_0)\right]. \tag{5}$$

The additional acceleration caused by the rotational motion includes centripetal, tangential, and Coriolis accelerations. Because the direction of the Coriolis acceleration is always perpendicular to the flow direction of the coolant and the RELAP5 code is a one-dimensional system code, the effects of the Coriolis acceleration on the coolant flow are negligible in the modified RELAP5 code.

The tangential acceleration $\overrightarrow{a_{\rm t}}$ is calculated as

$$\overrightarrow{a_{\rm t}} = \vec{\beta} \times \vec{r} = \beta\vec{n} \times \vec{r}. \tag{6}$$

The centripetal acceleration $\overrightarrow{a_{\rm C}}$ is calculated as

$$\overrightarrow{a_{\rm C}} = \vec{\omega} \times (\vec{\omega} \times \vec{r}) = \omega^2\vec{n} \times (\vec{n} \times \vec{r}), \tag{7}$$

where $\overrightarrow{n}$ is the unit vector of the rotation axis, and $\overrightarrow{r}$ is the space vector of the system component relative to the rotation axis, which can be obtained by multiplying the rotation matrix and the initial space vector $\overrightarrow{r}$ of the system component.

Therefore, the total additional acceleration due to ocean conditions can be expressed as

$$\vec{a} = \overrightarrow{a_{\rm l}} + \overrightarrow{a_{\rm t}} + \overrightarrow{a_{\rm C}}. \tag{8}$$

3 Modification of ocean condition models

3.1 RELAP5 code modification

The RELAP5 code is a large-scale transient thermal–hydraulic calculation program developed by the Idaho National Engineering Laboratory. A one-dimensional, transient, two-fluid, and six-equation hydrodynamic model is employed in RELAP5/MOD3.3. The RELAP5 code is widely used in the transient simulation calculations and safety analyses of reactor coolant system during accidents [21].

The two-fluid six-equation hydrodynamic model of the RELAP5 code comprises a two-phase continuity equation, two-phase energy conservation equation, and two-phase momentum conservation equation. The effects of the spatial position change and additional acceleration caused by ocean motion are primarily exerted on the body force term of the two-phase momentum conservation equation.

The momentum conservation equations of RELAP5 are calculated in the "vexplt" subroutine and can be expressed as

$$\begin{aligned} &\alpha_{\rm g}\rho_{\rm g}A\frac{\partial v_{\rm g}}{\partial t} + \frac{1}{2}\alpha_{\rm g}\rho_{\rm g}A\frac{\partial v_{\rm g}^2}{\partial x} = \\ &-\alpha_{\rm g}A\frac{\partial P}{\partial x} + \alpha_{\rm g}\rho_{\rm g}B_xA - \left(\alpha_{\rm g}\rho_{\rm g}A\right)FWG(v_{\rm g}) + \Gamma_{\rm g}A\left(v_{\rm gI} - v_{\rm g}\right) \\ &-\left(\alpha_{\rm g}\rho_{\rm g}A\right)FIG(v_{\rm g} - v_{\rm f}) - C\alpha_{\rm g}\alpha_{\rm f}\rho_{\rm m}A\left[\frac{\partial\left(v_{\rm g} - v_{\rm f}\right)}{\partial t} + v_{\rm f}\frac{\partial v_{\rm g}}{\partial x} - v_{\rm g}\frac{\partial v_{\rm f}}{\partial x}\right], \end{aligned} \tag{9}$$

$$\begin{aligned} &\alpha_{\rm f}\rho_{\rm f}A\frac{\partial v_{\rm f}}{\partial t} + \frac{1}{2}\alpha_{\rm f}\rho_{\rm f}A\frac{\partial v_{\rm f}^2}{\partial x} = -\alpha_{\rm f}A\frac{\partial P}{\partial x} + \alpha_{\rm f}\rho_{\rm f}B_xA \\ &-(\alpha_{\rm f}\rho_{\rm f}A)FWF(v_{\rm f}) - \Gamma_{\rm g}A(v_{\rm fI} - v_{\rm f}) \\ &-(\alpha_{\rm f}\rho_{\rm f}A)FIF(v_{\rm f} - v_{\rm g}) - C\alpha_{\rm f}\alpha_{\rm g}\rho_{\rm m}A\left[\frac{\partial\left(v_{\rm f} - v_{\rm g}\right)}{\partial t} + v_{\rm g}\frac{\partial v_{\rm f}}{\partial x} - v_{\rm f}\frac{\partial v_{\rm g}}{\partial x}\right], \end{aligned} \tag{10}$$

where $\alpha_{\rm g}$ and $\alpha_{\rm f}$ are the void fraction of vapor and liquid, respectively; $\rho_{\rm g}$, $\rho_{\rm f}$, and $\rho_{\rm m}$ are the density of vapor, liquid, and mixture, respectively; $v_{\rm g}, v_{\rm f}, v_{\rm gI},$ and $v_{\rm fI}$ are the velocity of vapor, liquid, vapor interface and liquid interface, respectively; FWG and FWF are the wall drag coefficients of vapor and liquid, respectively; FIG and FIF are the interphase drag coefficients of vapor and liquid, respectively; $\Gamma_{\rm g}$ is the volumetric mass exchange rate of vapor, C the virtual mass coefficient, A the cross-sectional area, P the pressure, and B_x the body force in x coordinate direction.

The momentum conservation equation is calculated in the RELAP5 code in the form of sum and difference equations. The body force term is eliminated in the difference equation; therefore, only the body force term in the sum momentum equation must be considered. The sum momentum equation can be expressed as

$$\begin{aligned}\alpha_g\rho_g\frac{\partial v_g}{\partial t}+\alpha_f\rho_f\frac{\partial v_f}{\partial t}+\frac{1}{2}\alpha_g\rho_g\frac{\partial v_g^2}{\partial x}+\frac{1}{2}\alpha_f\rho_f\frac{\partial v_f^2}{\partial x}\\=-\frac{\partial P}{\partial x}+\rho_m B_x-\alpha_g\rho_g FWGv_g\\-\alpha_f\rho_f FWFv_f-\Gamma_g\left(v_g-v_f\right),\end{aligned}\tag{11}$$

where, $\rho_m B_x$ is the body force term, ρ_m the mixture density, and B_x the product of the gravitational acceleration g and vertical height Z of the volume.

After incorporating the effects of the spatial position change and additional acceleration caused by ocean conditions, the modified body force term can be expressed as follows:

$$\begin{aligned}\rho_m B_x&=\rho_m(\vec{g}-\vec{a})\cdot\overrightarrow{L_1}\\&=\rho_m\left[-a_x x_1-a_y y_1-(g+a_z)z_1\right],\end{aligned}\tag{12}$$

where $a_x, a_y,$ and a_z are the additional accelerations in the x-, y-, and z-directions, respectively; $x_1, y_1,$ and z_1 are the new spatial position coordinates of the volume.

An ocean condition parameter input card was used to input the required ocean motion parameters into the RELAP5 code. For rotational motion, the unit vector of the rotation axis, the coordinates of a volume relative to the rotation axis, the volume number, and the period and amplitude of the rotation angle are input. For linear motion and static inclinations, the input parameters are relatively simple.

RELAP5 calculates the loop spatial position in the "ielvtn" subroutine, in which the spatial position of each loop volume relative to the rotation axis is calculated. Using the coordinates of the input volume relative to the rotation axis, the space vector $\vec{r}$ of all volumes relative to the rotation axis can be calculated. Based on Eqs. (6) and (7), the effect of rotation motion on each volume can be calculated in the "vexplt" subroutine.

The modified RELAP5 code can realize the input and calculation of the three basic ocean movement forms to simulate the parameter changes and system response of the reactor system and components under ocean conditions.

3.2 Code validation

Ishida established a natural circulation experiment under moving conditions to verify the modified RETRAN-02 code used to simulate a marine reactor [12]. In this study, the modified RELAP5 code was verified using the two-loop natural-circulation experimental platform established by Ishida. To verify the code, the calculation data of the modified RELAP5 code were compared with the experimental data of Ishida [12] and the simulation results of Cheng et al. [16].

The experimental platform comprised two coolers, a heater, and a pressurizer, as shown in Fig. 1a. Using the driving force provided by the density difference, a two-loop natural circulation flow with bilateral symmetry was formed. The operating pressure of the system was 0.1 MPa. The total power of the heater was approximately 60 kW.

Figure 1b shows the natural circulation mass flow rate at different inclination angles. The experimental setup was inclined counterclockwise. As the inclination angle increased, the height difference between the heater and cooler of the left loop decreased, and the driving force of the left loop decreased, resulting in a decrease in the left flow. Meanwhile, the height difference between the heater and cooler of the right loop increased, the driving force of the right loop increased, resulting in an increase in flow on the right side. Because the driving force of the overall natural circulation decreased, the total flow decreased as well. When the inclination angle reached 60°, the flow of natural circulation on the left loop decreased to 0. The average absolute error between the simulation results and Ishida's experimental data was 6.70%, which was within the acceptable range, thus verifying the capacity of the modified RELAP5 code for simulating the inclining condition.

Figures 1c, d show the average, maximum, and minimum values of the total natural circulation flow under different periods and amplitudes of the heaving motion. As the period and amplitude increased, the fluctuation amplitude of the flow increased gradually, whereas the average flow rate remained unchanged. When the period of the heaving motion was large, the growth rate of the oscillation amplitude of the flow decreased. The simulation results were consistent with the conclusions of Ishida [12] and Cheng et al. [16].

Figure 1e shows the natural circulation flow under a rotation motion of amplitude 10° and period 10 s. Considering the bottom volume as the origin of the rotation axis, the direction of the rotation axis was along the positive direction of the Y-axis. Consistent with the conclusion in the literature [22], the phase difference between the mass flow fluctuations in the two cooling circuits was 180°, which did not significantly change the total flow rate through the heater.

3.3 Helical tube modeling and sensitivity analysis

The SG for the IRIS reactor was selected as the research object. A calculation model for the IRIS reactor of the HCOTSG was established in this study under ocean

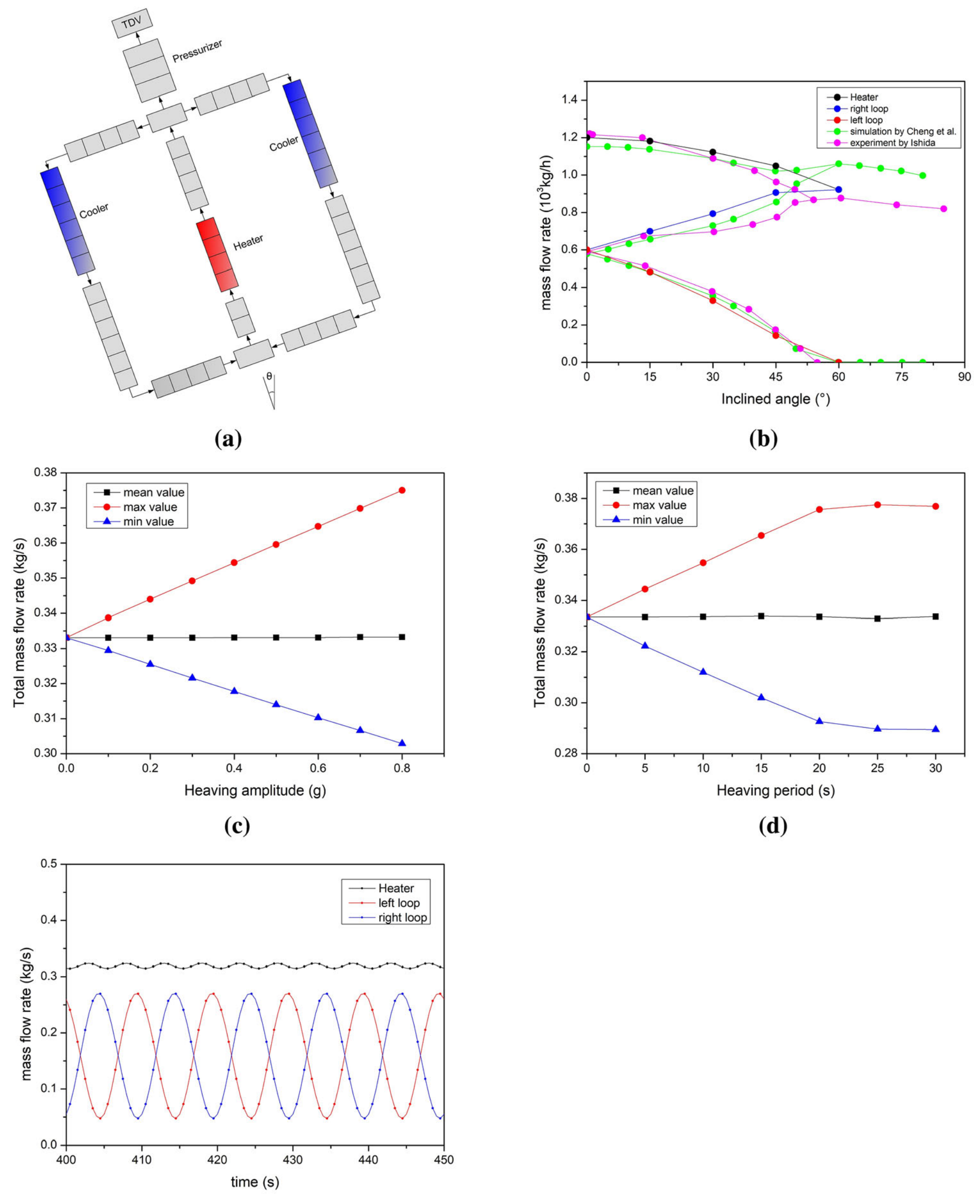

Fig. 1 (Color online) Simulation of natural circulation experiment: (**a**) RELAP5 nodalization. (**b**) Mass flow rate under static inclining. (**c**) Effects of heaving amplitude (T = 5 s). (**d**) Effects of heaving period (A = 0.3 g). (**e**) Mass flow rate under rolling condition (θ = 10°, T = 10 s)

conditions. Yan et al. designed a small FNPP based on the structure of the IRIS reactor to analyze the effects of ocean motion on the FNPP during an SBO accident [20]; however, a U-tube SG was used in the design loop.

The nodalization diagram of the IRIS reactor is shown in Fig. 2a. The IRIS comprised eight SGs, and only one of them is shown in the nodalization diagram for simplicity. The locations of the SGs and water storage tanks for the emergency heat removal system are shown in Fig. 2b. Pipes 414 and 514 are the primary and secondary sides of the SG, respectively. Table 1 lists the detailed parameters of the IRIS SG. When modeling the HCOTSG, an inclined tube is used as a simplification of the helical tube. The inclined and helical tubes have the same inclination angle, equivalent flow area, hydraulic diameter, heat transfer area, and vertical height. The heat transfer coefficient is multiplied by 1.1 to account for the heat transfer enhancement due to the centrifugal force of the helical tube [17, 23]. Therefore, the heat-transfer enhancement ability of the helical tube structure and swirling in the channel to the entire SG can be simulated. The primary side is equivalent to a vertical straight tube, as shown in Fig. 2c.

To simulate the effects of the helical tube structure on the coolant flow under ocean conditions, the horizontal direction of the helical tube was modeled as a periodic helical structure, as shown in Fig. 2d. The geometric size

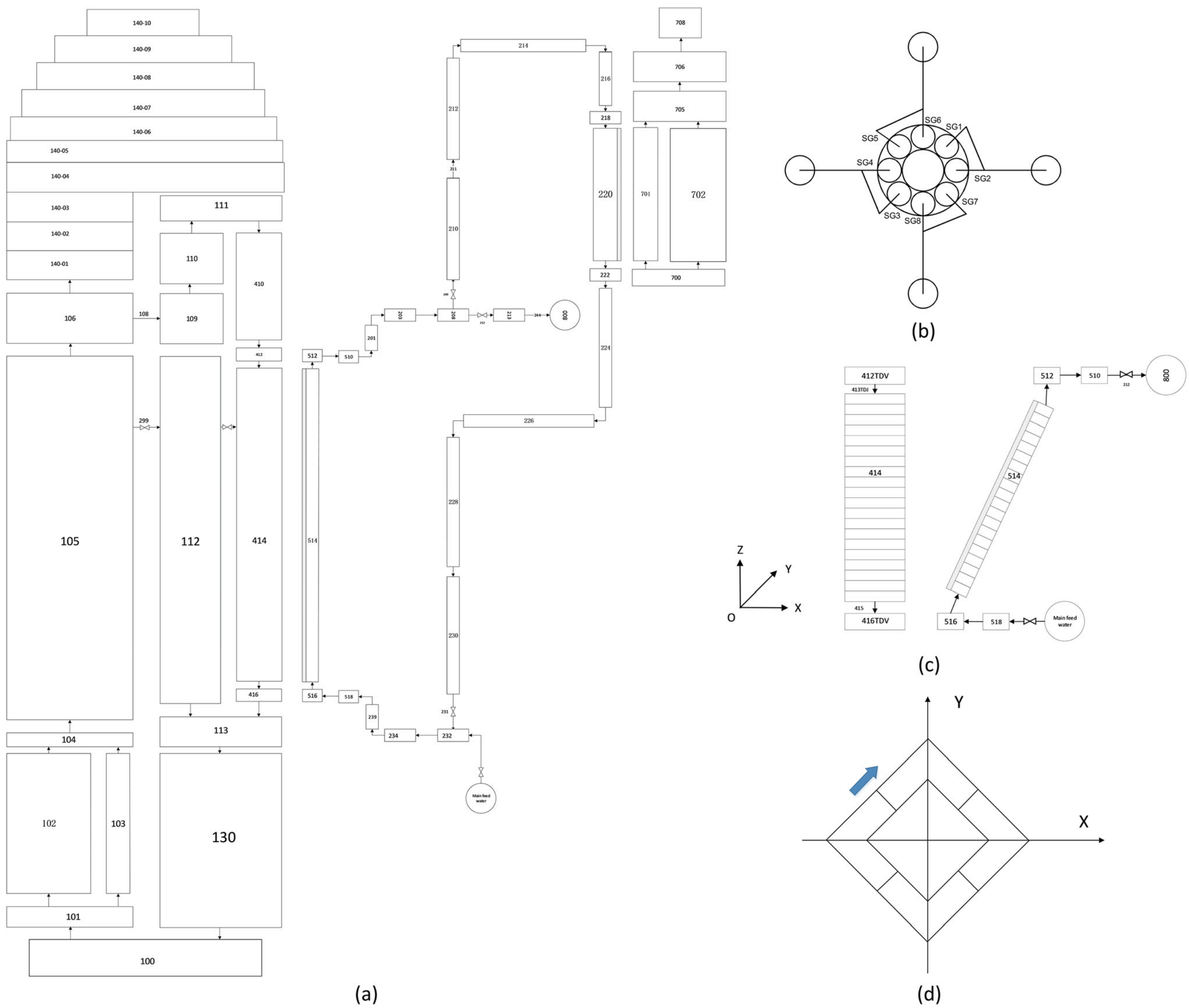

Fig. 2 RELAP5 nodalization diagram: (**a**) IRIS reactor. (**b**) Location of HCOTSGs and water storage tanks. (**c**) HCOTSG of IRIS reactor. (**d**) HCOTSG horizontal structure

Table 1 Detailed parameters of IRIS steam generator

Parameters	Value
Inlet temperature at primary side (K)	601.55
Outlet temperature at primary side (K)	565.29
Pressure at primary side (MPa)	15.5
Mass flow rate at primary side (kg/s)	589
Inlet temperature at secondary side (K)	497.05
Outlet temperature at secondary side (K)	592.35
Pressure at secondary side (MPa)	5.8
Mass flow rate at secondary side (kg/s)	62.5
Height of steam generator (m)	8.2

and number of cycles of the helical structure were used as the average values of those of an actual helical coil. In the RELAP5 code, the horizontal position of the pipe does not affect the calculation results [21]; thus, horizontal helical structure modeling does not affect the simulation calculation of the HCOTSG under normal conditions but can reflect the effect of the helical tube structure on the flow under ocean conditions.

Figure 3 shows the node number sensitivity analysis performed on the HCOTSG. The number of nodes did not significantly affect the pressure and temperature of the SG. When the number of nodes was 80, the parameters of the SG changed slightly. In other words, the calculation result was independent of the number of nodes at that instant. Therefore, the HCOTSG was modeled using 80 nodes in the simulation.

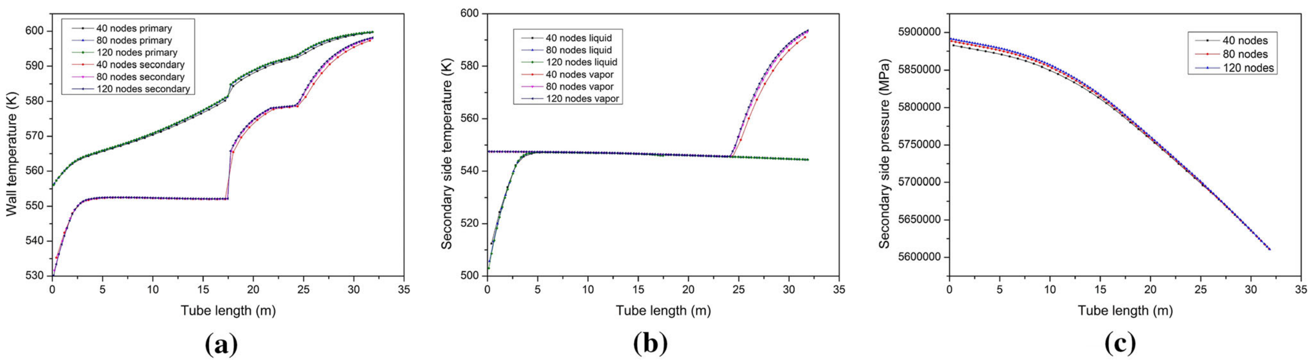

Fig. 3 (Color online) Parameters of HCOTSG with different number of nodes. (**a**) Secondary-side pressure drop. (**b**) Secondary-side temperature. (**c**) Wall temperature

4 Forced circulation characteristics under rolling motion

During the forced circulation operation of the reactor, the pump operated normally, and the driving force of the coolant was primarily provided by the pump; thus, ocean conditions did not significantly affect the primary and secondary circuits. The HCOTSGs at symmetric positions exhibited opposite fluctuations in the flow rate of the primary coolant and can reduce the effects of ocean conditions on the primary circuit. Therefore, the flow oscillation in the primary circuit during forced circulation did not significantly affect the HCOTSG. As shown in Fig. 2c, the boundary conditions at the primary side of the HCOTSG can be specified using 412,416 time-dependent volumes and 413 time-dependent junctions. Similar specifications were used for the secondary side, and the boundary conditions were determined by the time-dependent volumes and junctions.

The rotation axis was set at 1 m directly below the SG, and its direction was along the positive direction of the *Y*-axis. The rolling motion period was 10 s, and the amplitude was 15°.

4.1 Effect of flow rate

The heat transfer zones on the secondary side were distributed along the axial direction, including the subcooled liquid, gas–liquid mixing, liquid-deficient, and superheated steam zones [4]. When the IRIS reactor was operating at full power, the mass flow at the secondary side of the HCOTSG was 62.5 kg/s. $\Delta\max$ and $\Delta\min$ are used to represent the fluctuation amplitude of the heat flux and can be expressed as

$$\Delta\max = \frac{q_{\max} - q\mathrm{ave}}{q\mathrm{ave}}, \tag{13}$$

$$\Delta\min = \frac{q\mathrm{ave} - q_{\min}}{q\mathrm{ave}}, \tag{14}$$

where q_{ave}, $q_{\max}$, and $q_{\min}$ are the average, maximum, and minimum values of the heat flux under rolling motion, respectively.

Figure 4a shows the axial distribution of the heat flux on the secondary side of the SG at full power. The average value of the heat flux under rolling motion was the same as that in the steady state, and the fluctuation amplitude of the heat flux in the superheated steam zone was greater than that in the gas–liquid mixing zone.

Figure 4b shows the axial distribution of the heat flux on the secondary side of the SG when the mass flow on the secondary side of the SG was 23 kg/s. Because of the decrease in the mass flow rate, the length of the liquid-deficient zone in the SG decreased, and the superheated steam zone appeared in advance. The length of the liquid-deficient zone reduced from 6.8 to 2.4 m. In addition, the maximum fluctuation amplitude of the heat flux in the HCOTSG under rolling conditions increased from 0.96% to 5.8%.

Next, Δm is defined to represent the oscillation amplitude of the mass flow and can be calculated as

$$\Delta m = \frac{m_{\max} - m_{\min}}{2m_{\mathrm{ave}}}, \tag{15}$$

where m_{ave}, $m_{\min}$, and $m_{\max}$ are the average, minimum, and maximum values of the mass flow rate under rolling motion, respectively.

Figure 4c shows the axial distribution of the flow oscillation amplitude in the HCOTSG. As the mass flow decreased, the flow oscillation amplitude increased. Moreover, the smaller the mass flow, the greater the change in the oscillation amplitude. Figure 4d shows that the lower the flow rate, the higher the pressure drop at the SG. Therefore, the smaller the driving force at the helical tube side, the greater the fluctuation amplitude of the parameters at the HCOTSG and the greater the effects of the rolling conditions.

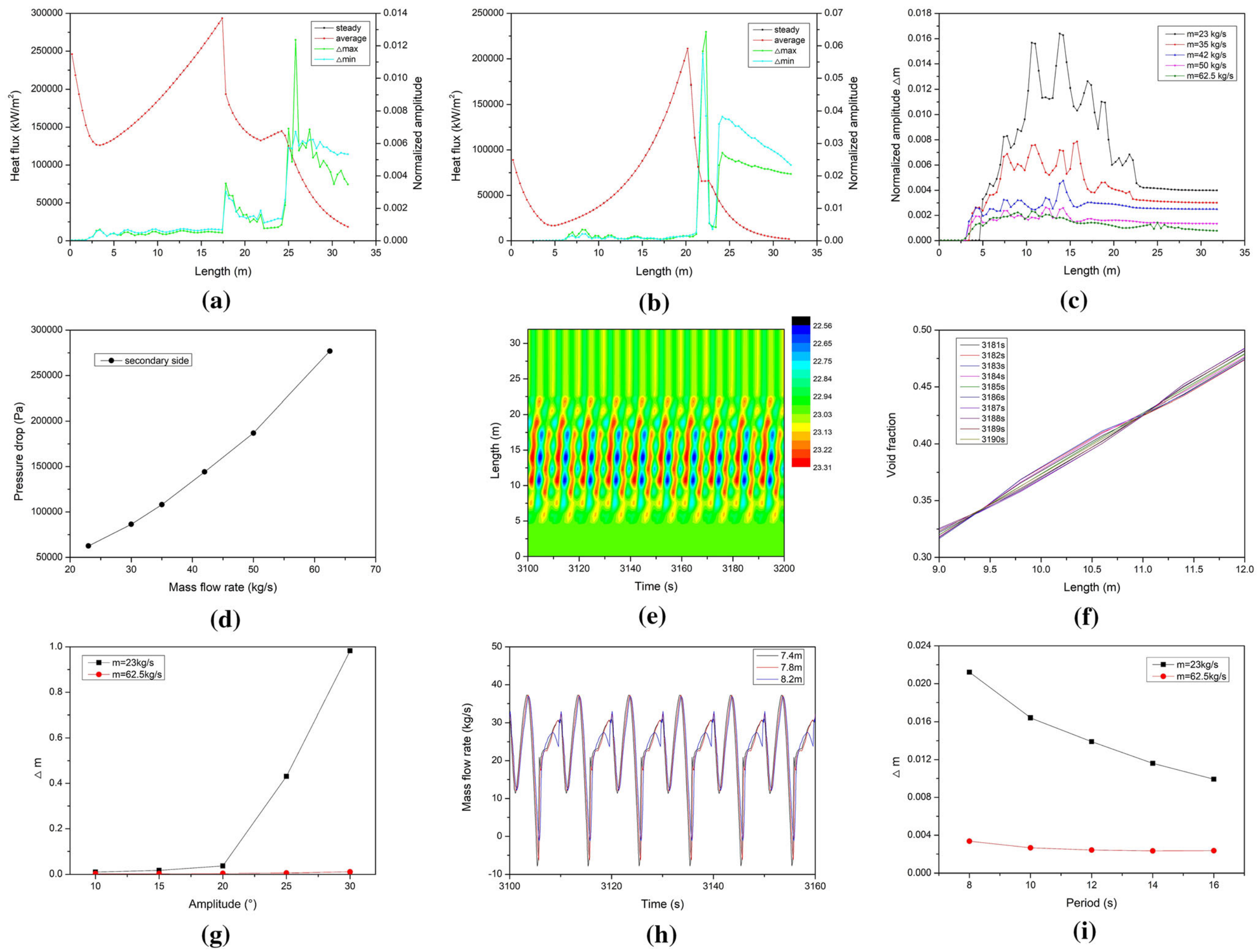

Fig. 4 (Color online) Parameters of HCOTSG under forced circulation. (**a**) Heat flux distribution ($m = 62.5$ kg/s). (**b**) Heat flux distribution ($m = 23$ kg/s). (**c**) Flow oscillation amplitude. (**d**) Pressure drop. (**e**) Secondary-side axial mass flow rate. (**f**) Void fraction at different times. (**g**) Effects of rolling angles. (**h**) Mass flow rate (amplitude 30°, period 10 s). (**i**) Effects of rolling periods

4.2 Effect of HCOTSG horizontal position

Based on the mass flow on the secondary side of the HCOTSG (i.e., 23 kg/s), the effect of the horizontal position was calculated and analyzed. Figure 4e shows the axial mass flow of the helical tube. The momentum conservation equation indicates that the additional forces on the gas and liquid phases are different; therefore, the oscillation amplitude in the gas–liquid mixing zone is the largest. Owing to the periodic horizontal structure of the helical tube, the coolant in the pipe can be affected by periodic additional tangential accelerations under rolling conditions; thus, the flow oscillation along the horizontal position changes periodically. Based on Eq. (6), the tangential acceleration a_t is directly proportional to the distance r from the volume to the rotation axis, and the rotation axis is directly below the HCOTSG. Therefore, the additional tangential force on the coolant increases along the axis; consequently, a phase difference exists in the flow oscillation along the axis. The time delay between the flow oscillation in the subcooled liquid and superheated steam zones was approximately 3.9 s.

Figure 4f shows the fluctuation difference in the void fraction with the change in the horizontal position of the helical tube. The void fraction at the central symmetry of the horizontal position fluctuates inversely, such as at 9.8 and 11.4 m, whereas the void fraction fluctuated only slightly at two symmetrical positions. At these two positions, the horizontal positions $y = 0$ and x exhibit the maximum and minimum values, and the effect of the additional force on the void fraction was offset. The change trend of coolant density was similar to that of void fraction. As the horizontal position changed, the fluctuation in the coolant density exhibited a periodic phase difference.

4.3 Effects of rolling angle and period under forced circulation

A change in the rolling motion parameters can affect the operation of the HCOTSG. Considering the maximum oscillation amplitude of the axial flow, Fig. 4g shows that the flow oscillation amplitude increased with the rolling angle. When the mass flow on the secondary side of the SG was 23 kg/s and the rolling angle was 30°, local countercurrent occurred at the HCOTSG, as shown in Fig. 4h. Therefore, during low mass flow forced circulation, a large rolling angle can cause a local countercurrent in the gas–liquid mixing zone of the HCOTSG.

As the rolling period increased, the flow oscillation amplitude and the rate of change decreased, as shown in Fig. 4i.

5 Natural circulation characteristics under rolling motion

Figure 2a shows that when the secondary circuit operates in natural circulation, the rolling motion periodically changes the height difference between the heater and cooler, thereby affecting the natural circulation drive head. The flow rates of the primary and secondary circuits decrease owing to pump shutdown during natural circulation. Therefore, rolling motion can exert a complex effect on the flow of the HCOTSG during natural circulation. The period of the rolling motion was 10 s, and the amplitude was 15°.

5.1 Effect of primary- and secondary-side coupling

When the primary circuit is under natural circulation, the rolling motion can affect the flow on the primary side of the HCOTSG, thus affecting the flow on the helical tube side. When an SBO accident occurs, the steam turbine is shut down, the main feed water is lost, the main pump is idle, the reactor is shut down, the passive emergency residual heat removal system begins to operate, and the primary and secondary circuits begin to operate in natural circulation.

Each passive system was connected to an HCOTSG. An SBO accident occurred at 100 s, and the rolling condition was introduced for analysis at 3000 s. The rotation axis was set at the bottom of the reactor core, and its direction was along the positive direction of the *Y*-axis. The rolling motion period was 10 s, and the amplitude was 15°.

The mass flow on the secondary side of the SG during the accident is illustrated in Fig. 5a. Owing to the change in the spatial position and the different effects of centripetal acceleration on the hot ascending and cold descending sections of the coolant, the average flow of the primary circuit decreased, as shown in Fig. 5b.

The primary-side parameters of the HCOTSG at 3000 s were input into the simplified model, and the natural circulation rolling condition was analyzed only on the secondary side. The flow comparison results are presented in Fig. 5c. Because of the decrease in the average flow in the primary circuit, the trough of the flow oscillation in the actual model reduced by approximately 24.3%. Moreover, as shown in Fig. 5d, a small peak occurred in the inlet flow fluctuation of the HCOTSG in the actual accident model, which was induced by the reverse oscillation of the primary- and secondary-side flows in the actual model under rolling conditions. Therefore, the flow oscillation in the primary circuit can complicate the flow in the secondary circuit and intensify the effect of rolling motion on the helical tube.

5.2 Effects of rolling angle and period under natural circulation

Because the rolling motion exerts a greater effect on the HCOTSG during natural circulation than during forced circulation, changing the rolling parameters can cause greater changes in the flow of the HCOTSG. Figure 5e shows that the maximum flow oscillation amplitude increases with the rolling angle. When the rolling angle exceeds 20°, a local countercurrent will occur at the HCOTSG. The larger the rolling angle, the smaller the average flow. Meanwhile, a smaller rolling period results in a smaller average flow, as shown in Fig. 5f.

5.3 Effect of gravity drive head change

The average mass flow at the HCOTSG decreases because the average driving force of natural circulation decreases under rolling motion. Based on Fig. 6a, the mass flow at steady state was 8.71 kg/s, and the average mass flow under rolling motion was 8.62 kg/s. The average flow decreased by approximately 1.0%. The maximum flow oscillation amplitude during natural circulation was approximately 50.8%. In contrast to forced circulation, because of the change in the driving head of the natural circulation, the flow oscillation amplitude in the subcooled liquid zone at the inlet of the HCOTSG increased, and the flow oscillation amplitude in the superheated steam zone at the HCOTSG outlet remained small. The average pressure at the HCOTSG increased because of the decrease in the natural circulation average flow under rolling conditions, as shown in Fig. 6b.

Figure 6c shows that owing to the low natural circulation mass flow, the liquid in the helical tube transitioned rapidly to saturated steam after the dry-out point. The

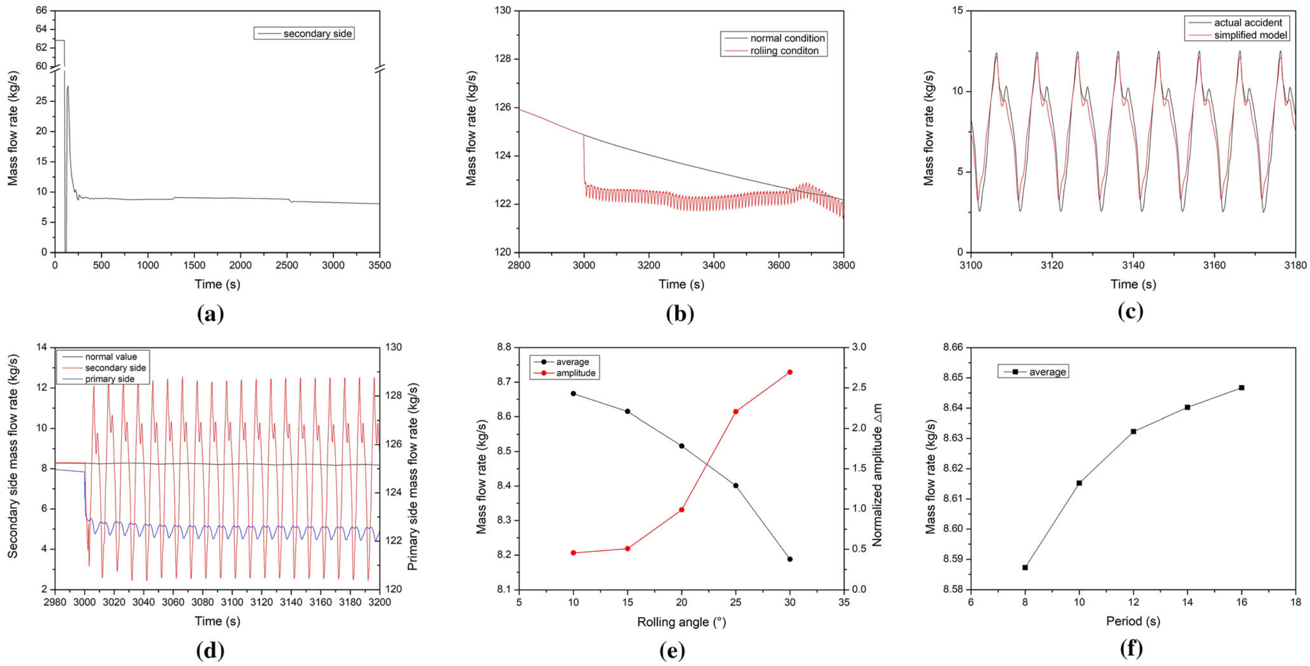

Fig. 5 Effects of rolling motion in SBO accident. (**a**) Secondary-side mass flow rate. (**b**) Primary-side mass flow rate. (**c**) Flow comparison between simplified model and SBO accident. (**d**) Mass flow rate under SBO accident (amplitude 15°, period 10 s). (**e**) Effects of rolling angles. (**f**) Effects of rolling periods

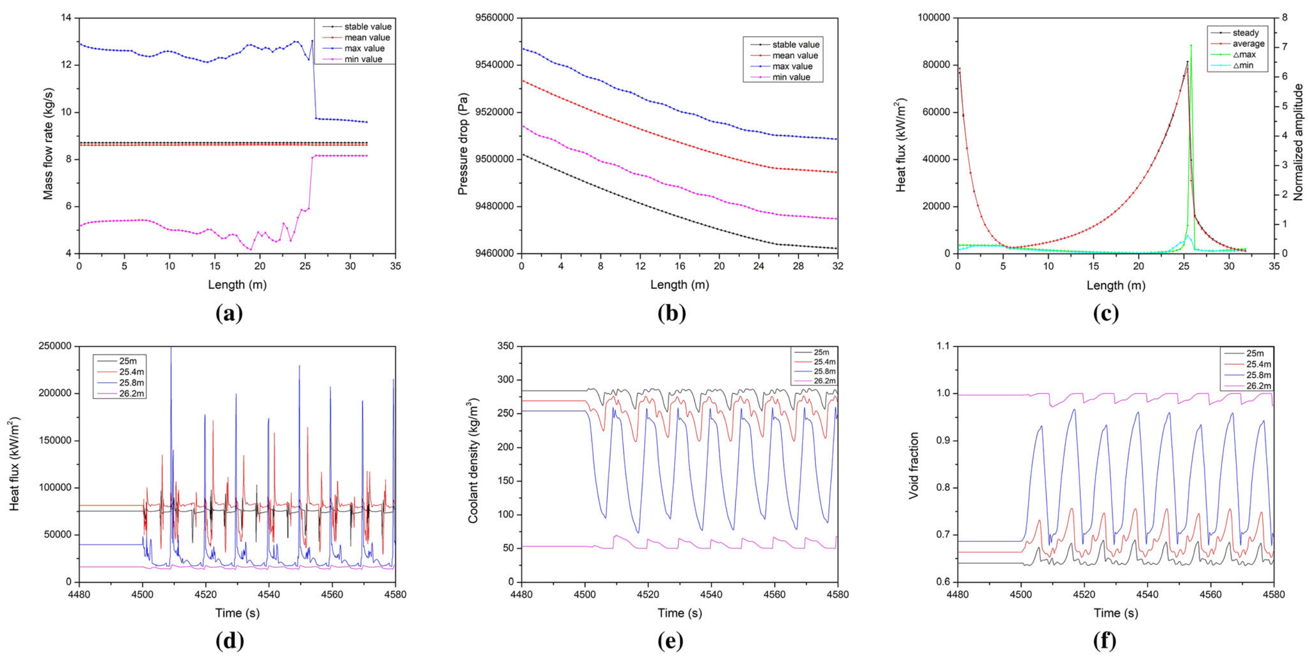

Fig. 6 (Color online) Parameters of HCOTSG under natural circulation: (**a**) Mass flow rate. (**b**) Pressure drop. (**c**) Axial heat flux distribution. (**d**) Heat flux at dry-out point. (**e**) Coolant density at dry-out point. (**f**) Void fraction at dry-out point

liquid-deficient zone disappeared almost completely. The rolling motion can affect the position of the dry-out point. In the steady state, the dry-out point was at 25.4 m. However, the dry-out point changed to between 25.0 and 25.8 m under rolling motion, as shown in Fig. 6d. Therefore, the coolant density and void fraction changed significantly at the dry-out point, and the average value under rolling motion was different from that under the steady state, as shown in Fig. 6e, f.

6 Conclusion

In this study, the theoretical model of ocean conditions was added to the RELAP5 code and verified using Ishida's experimental data. A three-dimensional RELAP5 model of the IRIS reactor and its HCOTSG was established, and the horizontal structure of the helical tube on the secondary side of the HCOTSG was simulated. The thermal–hydraulic characteristics of the HCOTSG under ocean conditions were calculated and analyzed using the modified RELAP5 code. The conclusions obtained are as follows:

(1) When the reactor was operating at full power, the flow oscillation amplitude at the HCOTSG was 0.27% under a rolling motion of amplitude 15° and period 10 s. As the forced circulation flow rate and rolling period decreased, and the rolling angle increased, the flow oscillation amplitude on the secondary side of the HCOTSG increased. In low flow forced circulation at a mass flow rate of 23 kg/s, a rolling motion with a rolling angle exceeding 30° can result in a local countercurrent in the gas–liquid mixing zone of the helical tube.

(2) During forced circulation, the effect of the rolling motion on the helical tube was primarily reflected in the additional tangential acceleration, which changed with the horizontal position. Therefore, in the gas–liquid mixing zone, the flow oscillation along the horizontal position changed periodically. Moreover, a phase difference of approximately 3.9 s at a flow rate of 23 kg/s flow rate was observed along the axial direction of the flow fluctuation. In single-phase liquid and single-phase gas zones, the effect of the rolling motion was insignificant.

(3) During the natural circulation on the secondary side of the HCOTSG, because of the change in height difference between the cooler and heater, the rolling motion affected the driving head of the natural circulation, resulting in a 1.0% decrease in the average flow rate and an increase in flow oscillation amplitude to approximately 50.8% under a rolling motion of amplitude 15° and period 10 s. Additionally, the relative flow oscillation amplitude in the subcooled-liquid zone at the SG inlet increased. As the flow rate decreased, the distribution of the heat transfer zones in the HCOTSG changed. The length of the liquid-deficient zone in the SG decreased, and a superheated steam zone appeared in advance. The position of the dry-out point changed as well.

(4) When an SBO accident occurred, the primary and secondary circuits began to operate in natural circulation. Under rolling motion, the flow oscillation on the primary side affected the heat transfer of the SG, thus rendering the flow oscillation on the helical tube side more complex. The trough of the flow oscillation reduced by approximately 24.3% under a rolling motion of amplitude 15° and period 10 s. As the rolling amplitude increased and the rolling period decreased, the average flow rate on the secondary side of the HCOTSG decreased.

Authors contribution All authors contributed to the study conception and design. Material preparation, data collection and analysis were performed by Tian-Ze Bai and Chang-Hong Peng. The first draft of the manuscript was written by Tian-Ze Bai and all authors commented on previous versions of the manuscript. All authors read and approved the final manuscript.

References

1. S.P. Wang, B.W. Yang, Z.B. Zhou et al., Review on thermal-hydraulic characteristics of nuclear reactors under ocean conditions. Nucl. Sci. Eng. **193**, 14–32 (2019). https://doi.org/10.1080/00295639.2018.1512791
2. X. Jie, Research Progress of Reactor thermal-hydraulic Characteristics under Ocean Conditions in China. Front. Energ. Res. **8**, 593362 (2020). https://doi.org/10.3389/fenrg.2020.593362
3. origination and direction of future development, V.M. Belyaev, M.A. Bol shukhin, A.N. Pakhomov et al., The world's first floating NPP. Atom. Energy. **129**, 27–34 (2020). https://doi.org/10.1007/s10512-021-00707-w
4. H. Yao, G. Chen, K.L. Lu et al., Study on the systematic thermal-hydraulic characteristics of helical coil once-through steam generator. Ann. Nucl. Energy **154**(3), 108096 (2021). https://doi.org/10.1016/j.anucene.2020.108096
5. H. Zhu, Z. Li, X. Yang et al., Flow regime identification for upward two-phase flow in helically coiled tubes. Chem. Eng. J. **308**, 606–618 (2017). https://doi.org/10.1016/j.cej.2016.09.100
6. I. Ishida, T. Kusunoki, H. Murata et al., Thermal-hydraulic behavior of a marine reactor during oscillations. Nucl. Eng. Des. **120**, 213–225 (1990). https://doi.org/10.1016/0029-5493(90)90374-7
7. S.C. Tan, G.H. Su, P.Z. Gao, Experimental study on two-phase flow instability of natural circulation under rolling motion condition. Ann. Nucl. Energy **36**, 103–113 (2009). https://doi.org/10.1016/j.anucene.2008.09.014
8. S.C. Tan, G.H. Su, P.Z. Gao, Experimental and theoretical study on single-phase natural circulation flow and heat transfer under rolling motion condition. Appl. Therm. Eng. **29**, 3160–3168 (2009). https://doi.org/10.1016/j.applthermaleng.2009.04.019
9. S.C. Tan, G.H. Su, P.Z. Gao, Heat transfer model of single-phase natural circulation flow under a rolling motion condition. Nucl. Eng. Des. **239**, 2212–2216 (2009). https://doi.org/10.1016/j.nucengdes.2009.05.002
10. C. Wang, X.H. Li, H. Wang et al., Experimental study on single-phase heat transfer of natural circulation in circular pipe under rolling motion condition. Nucl. Eng. Des. **27**, 497–504 (2014). https://doi.org/10.1016/j.nucengdes.2014.03.045
11. Z.T. Yu, S.C. Tan, H.S. Yuan et al., Experimental investigation on flow instability of forced circulation in a mini-rectangular channel under rolling motion. Int. J. Heat Mass Transf. **92**, 732–743 (2016). https://doi.org/10.1016/j.ijheatmasstransfer.2015.09.048

12. T. Ishida, I. Tomiai, *Development of analysis code for thermal hydro-dynamics of marine reactor under multi-dimensional ship motions, RETRAN-02/GRAV. Improvement of RETRAN-02 and experimental analyses* (Japan Atomic Energy Research Inst, Tokyo, 1992)
13. J.H. Kim, G.C. Park, Development of RETRAN-03/MOV code for thermal-hydraulic analysis of nuclear reactor under moving conditions. J. Korean Nucl. Soc. **28**(6), 542–550 (1996)
14. B.H. Yan, L. Yu, The development and validation of a thermal hydraulic code in rolling motion. Ann. Nucl. Energy **38**, 1728–1736 (2011). https://doi.org/10.1016/j.anucene.2011.04.007
15. H.J. Gong, X.T. Yang, Y.P. Huang et al., The development and validation of a natural circulation analysis code for marine reactors. J. Nucl. Sci. Technol. **54**, 500–512 (2017). https://doi.org/10.1080/00223131.2016.1262295
16. K. Cheng, T. Meng, F.L. Zhao et al., Development and validation of a thermal hydraulic transient analysis code for offshore floating nuclear reactor based on RELAP5/SCDAPSIM/MOD34. Ann. Nucl. Energy **127**, 215–226 (2019). https://doi.org/10.1016/j.anucene.2018.12.004
17. A. Cioncolini, A. Cammi, C. Lombardi et al., Thermal hydraulic analysis of IRIS reactor coiled tube steam generator. In: Proc. ANS M&C 2003 Topical Meeting, Paper 129, Gatlinburg, USA, April 6–11. (2003)
18. Z.Y. Xu, M.L. Liu, Y. Xiao et al., Development of a RELAP5 model for the thermo-hydraulic characteristics simulation of the helically coiled tubes. Ann. Nucl. Energy **153**, 108032 (2021). https://doi.org/10.1016/j.anucene.2020.108032
19. X.J. Li, T.L. Cong, Y.R. Chen et al., Research on backflow characteristics in U-tube of forced circulation steam generator under ocean conditions. Prog. Nucl. Energy **140**, 103894 (2021). https://doi.org/10.1016/j.pnucene.2021.103894
20. Q.Q. Yan, S.M. Luo, Y.P. Zhang et al., Effect of single and combined ocean motions on a small OFNP under SBO accidents. Ann. Nucl. Energy **145**, 107564 (2020). https://doi.org/10.1016/j.anucene.2020.107564
21. V.H. Ransom, J.A. Trapp, R.J. Wagner (ed.), *RELAP5/MOD33 Code manual volume I: code structure, system models, and solution methods* In: NUREG/CR-5535/Rev 1. Idaho National Engineering Laboratory, Idaho Falls (2001).
22. D. Li, R. Hao, Study on LOFA and LOHS accidents with passive safety system for integrated marine reactor. Nucl. Sci. Eng. **196**, 209–220 (2022). https://doi.org/10.1080/00295639.2021.1968760
23. A. Achilli, C. Congiu, R. Ferri et al., SPES3 facility RELAP5 sensitivity analyses on the containment system for design review. Sci. Technol. Nucl. Ins. **2012**, 173637 (2012). https://doi.org/10.1155/2012/173637